

## INFORMATION SCIENCE

## Millimeter-scale fluid-driven soft robots

Rong Bian<sup>1</sup>, Ninbin Zhang<sup>1</sup>, Xinyu Yang<sup>1</sup>, Jinhao Li<sup>1</sup>, Dezhi Yang<sup>1</sup>, Jieji Ren<sup>1</sup>, Jiang Zou<sup>1,2</sup> and Guoying Gu<sup>1,2,\*</sup>

## ABSTRACT

Millimeter-scale soft robots (milli-SRs) promise significant advancements in biomedical engineering and inspection, enabling precise navigation in confined spaces. However, fabricating miniaturized fluid-driven soft robots is hindered by microscale forces. Here, we introduce a new universal design and fabrication approach (termed as mini Bubble Casting method) to create high-quality multifunctional fluid-driven milli-SRs. By injecting a bubble into pre-modified silicone liquid under high-stability conditions, we achieve submillimeter internal voids, overcoming interfacial tension-induced instability. The modification strategy is guided by our theoretical model, which explains the influence of viscous resistance and interfacial tension on the dynamic behavior of the bubble-silicone interface. We successfully fabricate soft milli-actuators ten times smaller than existing works with low surface smoothness ( $R_a=11.2$  nm). We demonstrate a milli-gripper handling delicate insects and a thrombus extractor for narrow vessels. We present a miniature steerable tip for bronchial navigation, improving safety and dexterity over traditional tools, showing their tremendous biomedical potential.

**Keywords:** soft robotics | miniaturized robots | fluid dynamic | biomedical tools

## INTRODUCTION

Millimeter-scale soft robots (Milli-SRs), ranging from several millimeters down to hundreds of micrometers in size, are emerging as innovative tools in biomedical engineering and tissue inspection [1–7]. These robots can navigate through organs [1,8], grip objects [9,10], and transport medical devices and drugs [11] for diagnostics and therapy, offering minimally invasive access to the natural body cavities (Figure 1a). Milli-SRs can be actuated by various mechanisms, including pressure [12,13], electric field [14,15], magnetic field [16–18], chemical reaction [19,20], light [21], and ultrasound [22]. Among these, fluid-driven robots are particularly prevalent due to their ease of control and robustness [23–26]. A typical fluid-actuated soft robot comprises the silicone elastomer with one or more internal voids [27]. The pressure change in voids can be converted into deformation of soft robots. For biomedical applications, fluid-driven milli-SRs without external magnetic sources, enabling compact, lightweight medical devices [28]. Fabricated by non-metallic, MRI-compatible materials, they eliminate image

artefacts and enhance safety for both clinicians and patients [29,30]. Consequently, they are well-suited for complex endoluminal interventions [4], high-precision positioning [31], and environmental sensing [32] akin to magnetically driven milli-SRs.

While fluid-driven silicone robots at the centimeter scale are widely manufactured [33], fabricating their millimeter-scale counterparts remains challenging [34,35], especially in terms of robustness and stability, due to difficulties in creating smaller internal voids.

Structural defects and incompleteness frequently hinder the formation of millimeter-scale structures in traditional silicone molding methods. That is because the gravity and inertial forces, which dominate the molding process, are negligible compared to microscale forces in the low Reynolds number regime [35,36]. For example, in molding structures with a characteristic size of 1 mm, the Reynolds number is approximately  $10^{-3}$ . In this case, gravity fails to drive the silicone into the mold, and buoyancy is insufficient to lift the entrapped air. Moreover, the shapes and dimensions of robotic structures

<sup>1</sup>Robotics Institute and State Key Laboratory of Mechanical System and Vibration, School of Mechanical Engineering, Shanghai Jiao Tong University; Shanghai, 200240, China;

<sup>2</sup>Shanghai Key Laboratory of Intelligent Robotics, Shanghai Jiao Tong University, Shanghai 200240, China

\*Corresponding authors.

Email: [guguying@sjtu.edu.cn](mailto:guguying@sjtu.edu.cn).

Received: XX XX Year;

Revised: XX XX Year;

Accepted: XX XX Year

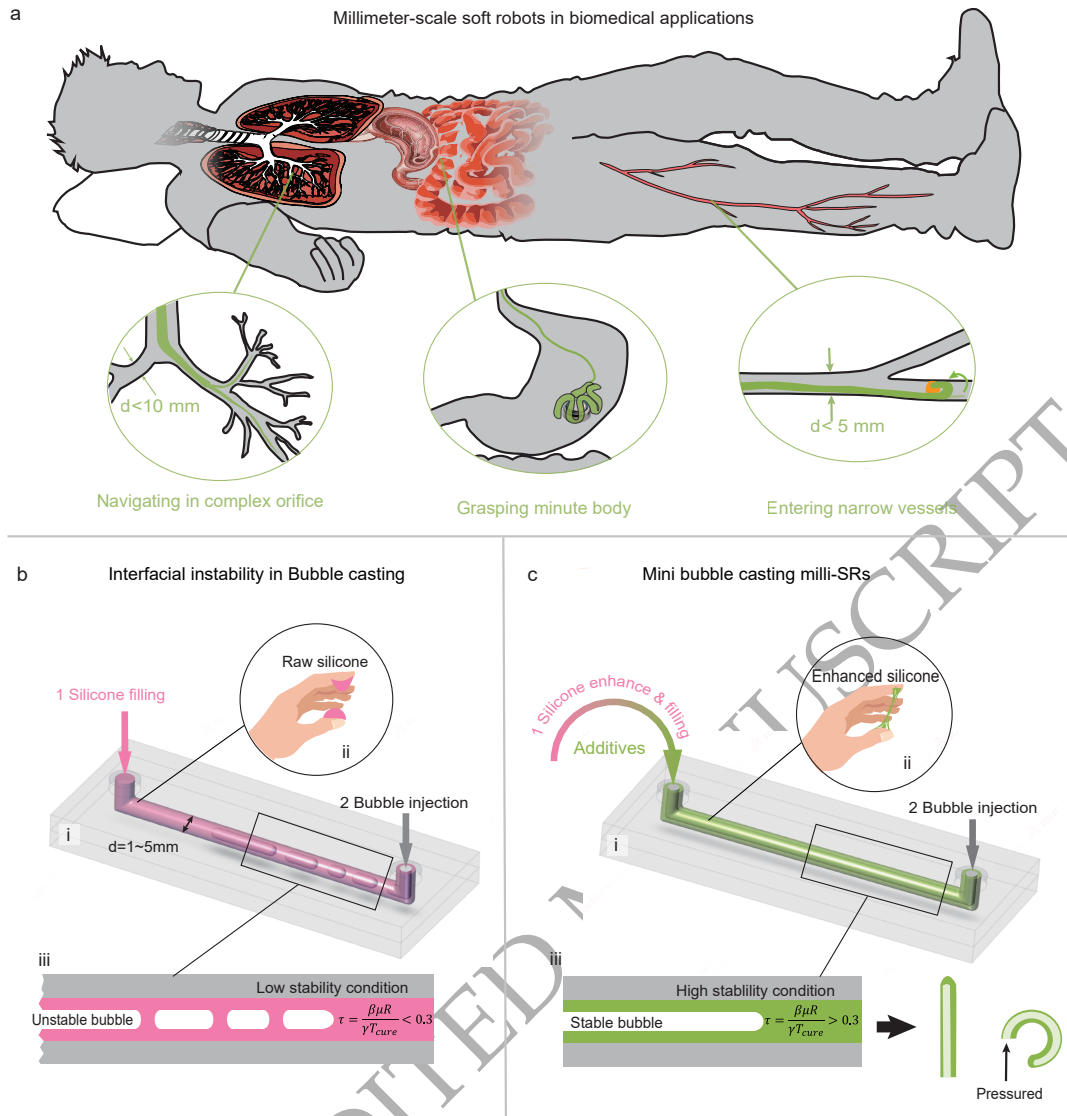


Figure 1: Concepts of milli-SRs and a comparison between Bubble Casting and Mini-BC. (a) Milli-SRs take on biomedical tasks in confined and narrow human cavities, including navigating in complex orifice, extracting foreign objects, and entering narrow vessels. (b) Interfacial instability in bubble casting milli-SRs. The bubble is injected into the raw silicone liquid to form a robot void. When the robot size is scaled down to the millimeter scale, the unmodified raw commercial silicone presents a low stability condition and cannot resist the microscale forces such as surface tension, resulting in interfacial instability. (c) Mini bubble casting enables the robust fabrication of milli-scale soft robots by enhancing silicone stability through incorporating additives, following universal strategies guided by our theoretical model. The enhanced silicone liquid with a high stability condition exhibits resistance to interfacial tension and the bubble remains stable until the milli-SRs are completed.

are restricted by the challenges associated with extracting long, narrow molds from the cured silicone [37]. Lately, other fabrication methods have been developed to enable novel mechanisms for mitigating failures induced by microscale forces; however, they encounter other problems. 3D printing faces limitations in material selection [38,39], and the film coating technique is also restricted to relatively simple ge-

ometries [40].

Recently, Bubble Casting [41] has emerged as a robust stable fabrication technique for manufacturing soft robots (Figure 1b, i). It leverages the interfacial flow within silicone liquid to create elongated robot voids [42,43]. Firstly, the liquid silicone is filled into a tubular mold, followed by bubble injection where the air is injected to form a long bubble in the silicone. The

ideal scenario is that the bubble stabilizes under mechanical equilibrium between viscous resistance, surface tension, and gravity. However, maintaining the stability of the bubble-silicone interface at the millimeter scale presents significant challenges. In experiments, we observe that the bubble fragments into a few discrete bubbles, and the silicone converges into peaks and forms bridges (Figure 1b, iii and Movie S1), which limits its ability to fabricate millimeter-scale robots. We hypothesize that this can be attributed to interfacial tension (Figure 1b, ii), which increases rapidly as the scale decreases, becoming significantly greater than the viscous resistance of silicone and gravity, thereby causing an imbalance in mechanical equilibrium [44–46]. This study elucidates the mechanism of interfacial instability and its mitigation method. Whereas conventional bubble casting [41] centers on bubble forming, our focus is on the milli-bubble fragmentation and on devising a robust strategy for the reliable fabrication of fluid-driven milli-SRs.

Herein, we present a novel universal robust fabrication method, Mini Bubble Casting (Mini-BC) to create fluid-driven silicone-based milli-SRs using various commercial liquid silicones (Figure 1c), extending the lower size limit of the Bubble Casting process. To explore the dynamic behavior of silicone liquid at the millimeter scale, we establish a theoretical model and identify the influence of the curing time, viscous resistance and interfacial tension on the interfacial instability. Based on the model, a rheological stability condition  $\tau$  is established and a universal modification strategy is proposed to enhance interfacial stability (Figure 1c, iii) by incorporating commercially available additives. The enhanced silicone  $\tau > 0.3$  can withstand interfacial tension (Figure 1c, ii), enabling theoretical minimal diameters of 0.2 mm. To illustrate its efficacy, a variety of soft actuators with different shapes and actuation modes are created, featuring dimensions one order of magnitude smaller than existing works [41,42], outer diameters ranging from 1.0 mm to 3.0 mm, and ultra-low surface roughness ( $R_a=11.2$  nm). We further demonstrate the capability of milli-SRs in interacting with delicate objects and navigating within narrow natural human orifices, including a compliant and biosafe insect gripper and thrombus extractor for vascular interventional surgery. Additionally, we present a miniature flexible steerable tip with omnidirectional bending capability of up to  $180^\circ$  that can navigate in complex bronchial environments and reach the quaternary bronchus, showcasing supe-

rior safety and dexterity compared to traditional medical tools. The proposed Mini Bubble Casting affords novel possibilities for fabricating soft robots at the millimeter scale, unlocking numerous potential applications in biomedical fields.

## RESULTS

### Interfacial instability in bubble casting

To demonstrate its broad relevance, we conduct preliminary experiments and observe interfacial instability across various commercially available liquid silicones, including the VPS series commonly used in Bubble Casting milli-SRs of varying diameters, as well as Ecoflex 30 and Dragon Skin 10 which are widely utilized in soft robotics laboratories (Figure 2a).

The interfacial instability can be categorized into four distinct stages in Figure 2b. Initially, in stage 1, the bubble undergoes subtle unevenness near point A, and then it forms a notable ‘hill’ in stage 2. The silicone continues converging to point A and the bubble is on the verge of fracture during stage 3. Ultimately, the silicone bridges form and the long bubble fragments into several smaller, isolated bubbles in stage 4, which marks the failure of bubble casting milli-SRs.

To model the dynamic behaviors, we first consider why silicone liquid converges to point A. In Figure 2c, the unevenness near point A creates a difference between the height of silicone layer at point A and point B, supposing  $h_A - h_B > 0$ . The Young-Laplace formula dictates that surface tension generates a pressure differential at point A, quantified as (see supplementary material ‘Young-Laplace formula’):

$$P_A - P_B = \gamma \left( \frac{1}{R - h_B} - \frac{1}{R - h_A} \right) < 0 \quad (1)$$

where  $\alpha$  is the surface tension coefficient between the silicone liquid and bubble, and  $R$  is the mold’s inner radius. Given that  $P_A - P_B < 0$ , the pressure gradient creates a pressure trap at point A that becomes deeper as the  $h_A$  increases. It makes the interface in an unstable equilibrium, initiating the subsequent instability on the bubble-silicone interface.

Then the silicone flow behavior can be obtained by formulating dynamic equations (see supplementary material ‘Navier-Stokes equation’), yielding during stage 1-3:

$$\frac{h_A}{h_0} = \left( 1 - \frac{\alpha \gamma h_0}{2\pi^2 R^2 \mu} t \right)^{-n} \quad (2)$$

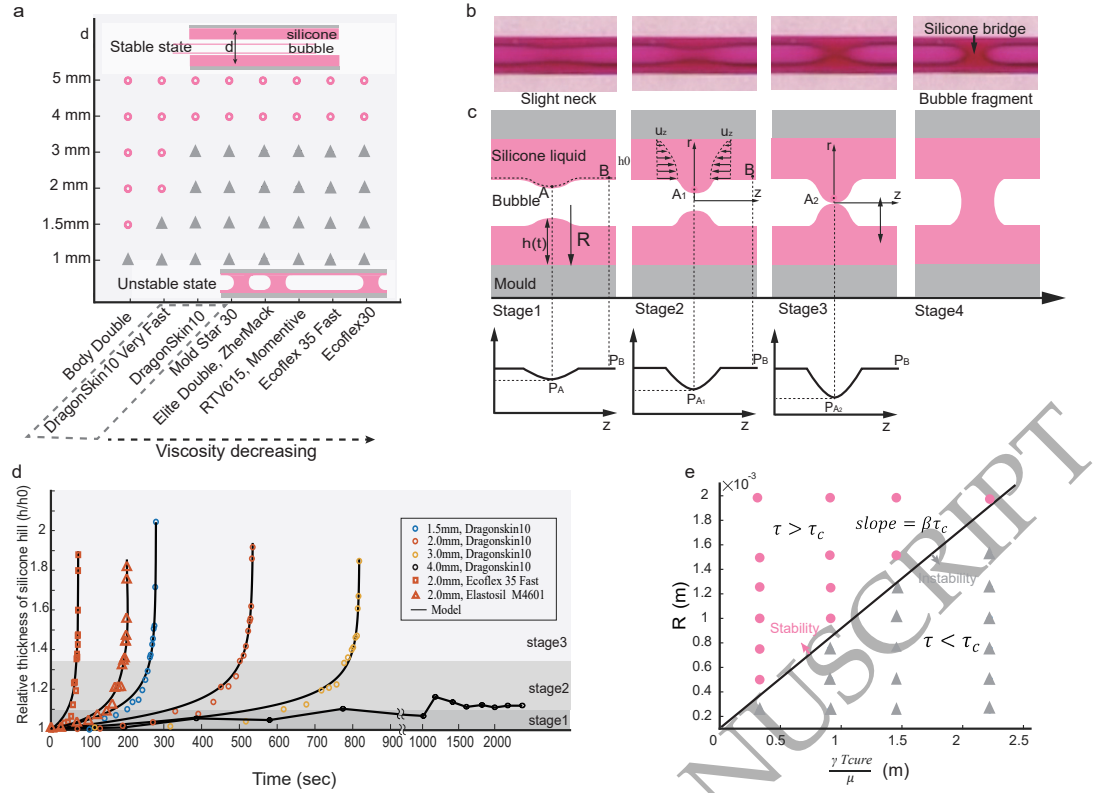


Figure 2: Model of interfacial instability. (a) Instability can be observed in the various commercial liquid silicones, including the VPS series used in Bubble Casting, as well as Ecoflex 30, and Dragon Skin 10 widely used in soft robotics laboratories. Silicones are arranged in descending viscosity; those of identical viscosity are grouped within dashed boxes. Their viscosities span 3 –100 Pa·s and covering the majority of commercially available silicones. (b) Four stages of interfacial instability from left to right. Diameter: 1.5 mm. (c) Diagram of silicone flow during the instability model, depicting the cross-section of the silicone liquid (pink) and the bubble (white) within a tubular mold (gray). At point A, the formation of a silicone hill creates a pressure trap, which subsequently induces the convergence of the surrounding silicone. (d) Dimensionless hill height  $h_A(t)/h_0$  versus time ( $t=0$  at bubble inception) for various diameters. The silicone liquid is Dragon Skin 10 (Smooth On Inc.), Ecoflex 35 Fast (Smooth On Inc.) and Elastosil M4601 (Wacker Inc.). Solid lines correspond to Equation (2) with fitted parameters (mean  $\pm$  s.e.): Dragon Skin 10:  $n = 0.0986 \pm 0.005$ ,  $\alpha = 0.12 \pm 0.04$ , Ecoflex 35 Fast:  $n = 0.112 \pm 0.006$ ,  $\alpha = 0.12 \pm 0.02$ , Elastosil M4601:  $n = 0.103 \pm 0.001$ ,  $\alpha = 0.13 \pm 0.01$ . Parameter explanation and fitting method are in supplementary material “Explanation of the fitting parameters”). (e) Occurrence of interfacial instability under varying silicone conditions and within molds of different radii. Solid circles  $\bullet$  indicate the stability and triangles  $\blacktriangle$  indicates the instability. The solid line classifies two states with the slope  $\beta\tau_{th}$ .

$$T_{grow} \approx \frac{2\pi^2\mu}{\alpha\gamma} \times \frac{R}{h_0} \times R \quad (3)$$

where  $T_{grow}$  is the instability timespan,  $h_0$  is the initial height of the silicone layer at point A,  $\mu$  is the silicone viscosity. This progression stops when  $h_A = R$  at stage 4, where the hill’s height reaches its maximum, breaking up the bubble. Figure 2d shows the growth of the dimensionless hill height  $h_i/h_0$  over time for various diameters and silicone types, demonstrating the close agreement with the theoretical equation [2].

According to the model results, the interfacial

instability is highly dependent on size and the rheological properties of silicone liquid. The instability timespan  $T_{grow}$  is positively correlated with the scale  $R$ . Furthermore, the growth velocity of height  $h_A$  correlates positively with the surface tension coefficient  $\gamma$ , and inversely with viscosity  $\mu$ . This explains the antagonistic effects of surface tension (promoting instability) and viscous forces (inhibiting instability).

### Instability condition and modification strategy

Determining whether instability occurs is another important aspect. To establish the instability condition, thought experiments are needed. It is noted that silicone liquid undergoes a viscosity increase and solidification during instability. Extreme stability happens when the silicone curing time  $T_{cure}$  is significantly shorter than the instability timespan  $T_{grow}$ , causing the silicone to instantly freeze after bubble creation. Conversely, another scenario of extreme instability is where  $T_{grow}$  is so small that the instability occurs rapidly in the uncured silicone. Therefore, the stability condition, denoted as  $\tau$ , can be established as:

$$\tau = \frac{T_{grow}}{T_{cure}} = \frac{\beta\mu R}{\gamma T_{cure}} \quad (4)$$

where  $\beta = \frac{2\pi^2}{\alpha} \times \frac{R}{h_0} \approx 329$ . A large  $\tau$  indicates high stability, while a small  $\tau$  corresponds to significant instability. Experiments validate the stability condition (Figure 2e) and the threshold criterion can be calculated as  $\tau_{th} = 0.3$  (see Methods ‘Stability condition’). The fabrication yield of mini bubble casting is quantified across various instability conditions and diameters (Radius=0.5-2.5 mm) to show the scalability of the proposed fabrication method. The improved fabrication yields confirm the scalability of the modification strategy (Figure S3).

Based on the stability condition, we can increase viscosity  $\mu$  and decrease curing time  $T_{cure}$  until  $\tau > \tau_{th}$  to mitigate interfacial instability. Notably, considering that the excessively high viscosity and rapid curing of silicone are detrimental to the operational process, the upper limitation of viscosity  $\mu_{max}$  is  $100 \text{ Pa} \cdot \text{s}$  and the low limitation of curing time  $T_{cure,min}$  is 10 min, which means the theoretical minimal diameter  $d_{min} = 0.2 \text{ mm}$  (see supplementary material ‘Theoretical minimal diameter by mini-BC’).

Figure 3a shows the modification strategy. Firstly, the commercial additives, thickeners and accelerators, are inserted into part A of silicone before both components are canned to injection cartridges. Take fabricating 1.5 mm soft actuators with Dragon Skin 10 as an example, the condition of the unmodified silicone  $\tau_0 \approx 0.05$ . Based on sheets from suppliers, we insert the thickener (Thi-Vex, Smooth-On Inc., 3% of part A) and the accelerator (Plat-Cat, Smooth-On Inc., 1% of part A in weight) into silicone A. The new condition in the mixed silicone liquid is  $\tau \approx 0.4$ . Then, the modified silicone is mixed in the mixing nozzle and injected into the mold.

After a waiting period, the air is injected from another side and forms a long bubble in the silicone liquid. Figure 3b shows the interfacial behaviors under different conditions. Silicone with high  $\tau$  shows interfacial stability. The process is shown in Movie S2. For other commercial silicone, the suggested additives and their dosage are listed in Table S1. Excluding silicone curing, total fabrication requires 10 min; including curing, the process spans 20–70 min (Table S2).

### Milli-SRs by mini bubble casting

We successfully fabricated various milli-SRs that are similar but an order of magnitude smaller than those by Bubble Casting. To demonstrate the stability of Mini-BC, a contractile coiling soft actuator ( $R = 0.75 \text{ mm}$ ,  $L = 300 \text{ mm}$ ) with aspect ratio  $L/R$  as high as 400 is created in Figure 3c and Movie S3 (its counterpart  $R = 5 \text{ mm}$  in Bubble Casting). Its contractile ratio of original length to minimal length can reach up to 8.5 times and it generates a contractile force of  $\approx 400 \text{ mN}$  (Figure S8). This millimeter-scale actuator can serve as a driver for micro-mechanical systems, analogous to the role of an electric motor in large-scale machinery. The contractile milli-actuator drives a microscale rotating pair lifting a minuscule paper clip (Figure 3d and Movie S3). The bending milli-actuator spins a milli-gear set (Figure 3e and Movie S4). We also create similar but smaller five-point star-shaped anisotropic actuators (Figure 3f and Movie S5) and cross-like actuators (Figure S2 and Movie S6). They are 10 mm in diameter and one order of magnitude smaller than their bubble-casting counterpart in size (80 mm in diameter).

The surface roughness of milli-SRs is measured at  $Ra=11.2 \text{ nm}$  using an atomic force microscope (MFP-3D, Oxford Instruments) equipped with a stylus tip radius of  $1.0 \mu\text{m}$ , as shown in Figure 3g. The roughness is several orders of magnitude smaller than its counterpart fabricated by casting ( $Ra=1-10 \mu\text{m}$  [47]), and 3D printing ( $Ra=6 \mu\text{m}$  [38]). We quantitatively evaluate the wall-thickness uniformity (Figure S4); details to ensure consistency are provided in supplementary material ‘The uniformity of the robot’s wall thickness’. The milli-SRs withstand a thousand loading cycles without any visible degradation in deformation performance (see supplementary material ‘Motion repeatability’, Figure S6). Mini-bubble casting is benchmarked against alternative fabrication routes in supplementary material ‘Comparative Benchmarking of Millimeter-Scale Fabrication Techniques’.

Due to their delicacy and inherent safety, the

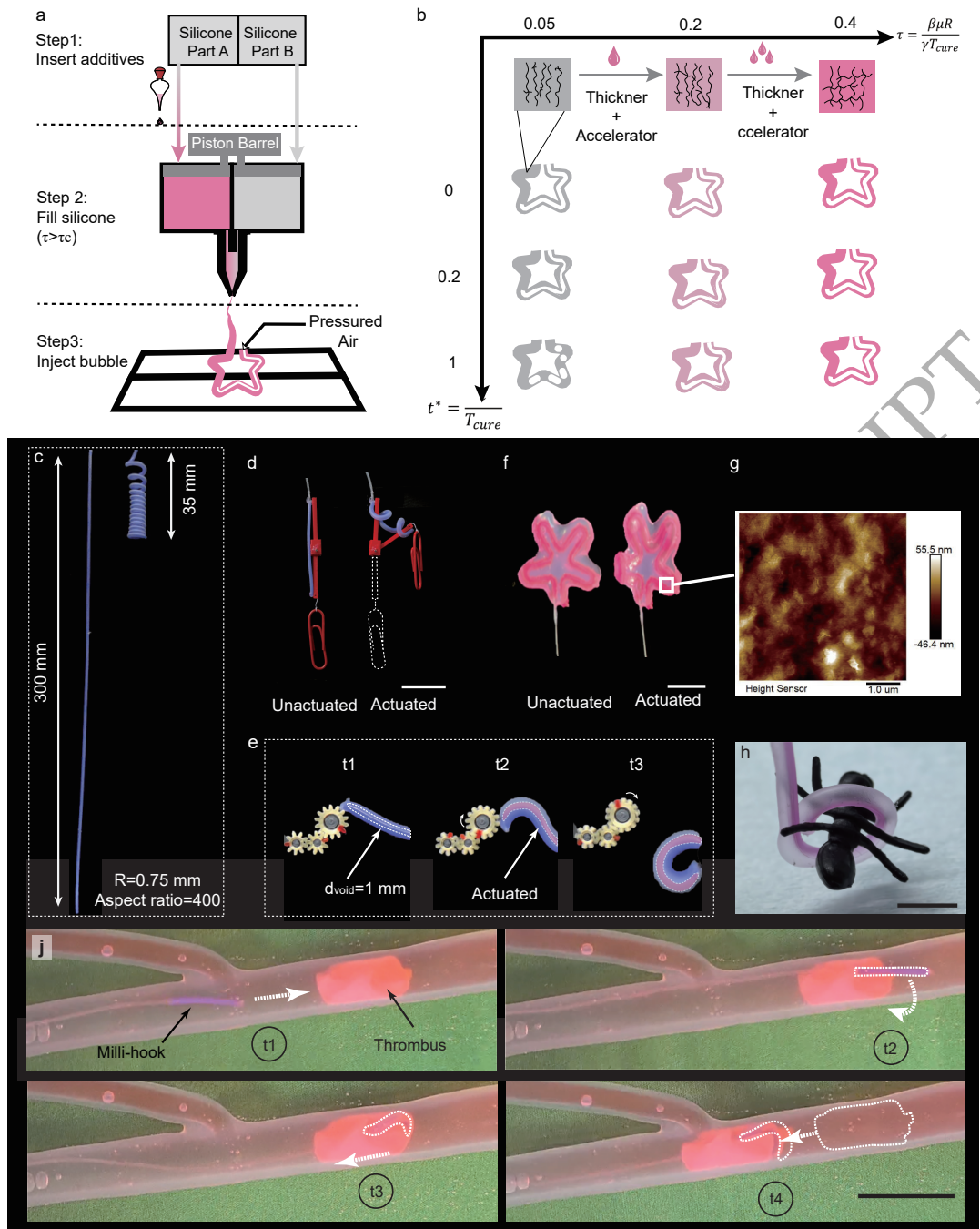


**Figure 3: Silicone modification and milli-SRs by mini-BC.** (a) Silicone modification strategy. (b) The interfacial behaviors as the dimensionless time  $t/T_{cure}$  when creating a starlike soft actuator with a diameter of 2 mm. From left to right, we add additives to modify its stability condition  $\tau$ . (c-e) Soft actuators similar in shape but smaller compared to those produced by Bubble Casting. (c) Contractile coiling of an actuator with a radius of  $R=0.75$  mm and  $L=300$  mm. (d) Muscle-like contraction of a soft actuator that drives a microscale rotating pair. Scale bar, 5 mm. (e) Series of images of bending actuator driving the milli-gear set. (f) A star-like actuator is attached to a thin membrane. Scale bar, 5 mm. (g) The atomic force microscope image of the void surface of the soft actuator. (h) A milli-gripper grasping and holding an ant model. Scale bar, 5 mm. (j) A milli-gripper with a bendable tip enters the vessel (inner diameter, 8 mm) and withdraws a thrombus simulator. Its contour is delineated with a dashed line for enhanced clarity. Scale bar, 10 mm.

milli-actuators are proficient in grasping tiny objects and entering narrow tubes. A soft bending actuator with 1.5 mm in diameter can function as a milli-gripper of microscale objects that are easily deformed and damaged by rigid grippers. The ant model is gripped and held without damaging its body (Figure 3g). Dislodgement of the ant from the milli-gripper requires a pulling force of  $\approx 220$  mN. (Figure S8). We can also create a soft milli-hook whose tip easily bends and body hardly deforms under a single pressure by programming the Mini-BC process (Figure S7). The hook penetrates the narrow canal, engages the foreign object, and withdraws it intactly (Figure 3j; Movie S7). Free from the external constraints, the deflected tip forms a precise circular arc (Figure S5) and we characterize its curvature–pressure relationship is quantified in supplementary material “Relationship between pressure and curvature”). All milli-SRs shown in Figure 3 are pneumatically actuated via compressed air supplied by a precision syringe pump (Figure S10).

### Biomedical application

Bronchoscopy is a common procedure for examining lung diseases, using a slender bronchoscope (2.2-6.3 mm) with a micro camera for clinical evaluation. Its steerable tip, controlled by multiple cables, allows precise navigation through the bronchial tree (Figure 4a). However, commercial bronchoscopy can cause complications like tissue damage and bleeding. To mitigate these risks, the use of soft materials presents an inherently safer alternative, reducing pain and promoting faster recovery.

Here, we designed an omni-curved bronchoscope tip composed of milli-actuators capable of reaching the quaternary bronchus (Figure 4b). The tip incorporates three 1.5-mm soft actuators fabricated by Mini-BC with Dragon Skin 10 (Smooth-On Inc.) and a micro camera (TA10, 720p, 0.65 mm  $\times$  0.65 mm) equipped with two miniature white LEDs. The actuators are arranged in parallel and glued together, with the camera fixed at the tip. Selective pressurization of individual chambers produces localized elongation, inducing deflection of the tip (Figure S9). For enhanced safety, normal saline is used as the pressurizing fluid in case of accidental explosion. The soft material, with a Young’s modulus of less than 150 kPa and demonstrated biocompatibility, minimizes the risk of tissue damage, ensuring the tip is gentle enough to navigate the bronchial walls without causing harm. It is dexterous with a maximum bending angle of 180°

(Figure S4d) that can meet the need for navigating in the bronchus.

To evaluate its potential for biomedical applications, we assess its capabilities to steer and detect in a realistic setting. A real-size, resin bronchus model, which accurately mimics the human bronchial environment, is used for this purpose. The model is transparent to allow for presentation (Figure 4c). The task of the soft bronchoscope is to insert into the main bronchi (d=15-17 mm, Figure 4c, i), bend on the right into the right lobar bronchi (d=4-10 mm, Figure 4c, ii), and reach the right lower lobar bronchus to examine the subsegmental bronchus (d=2-4 mm, Figure 4c, iii). The numbers are labeled on the end of the subsegmental bronchus and a special marker + is glued on the No.1 bronchus.

The path from the main bronchi to the right lower lobar bronchus spans diameters ranging from 17 mm to 4 mm, over a distance of 25 cm. In Figure 4c, iv-ix, we demonstrate experimentally our soft bronchoscope can complete this task (Movie S8). The operator holds the soft bronchoscope and manually manipulates the switch to adjust the inner pressure of milli-actuators. The operator can control the bending of the soft bronchoscope in the desired direction. The microcamera on the top of the soft bronchoscope detects the markers + near the No.1 branch in Figure 4c, iv as well as the marks of No.2-7 in Figure 4c, v-ix.

### DISCUSSION

This work elucidates and suppresses the interfacial instability in Bubble Casting milli-SRs, thereby pushing the attainable lower bound of the technique to the millimeter regime. Our study reveals that interfacial tension and viscous resistance act as antagonistic regulators of interfacial instability, a coupling previously unreported [37,41,42]. A dimensionless stability condition  $\tau$  is introduced to predict the onset of instability; guided by it, we further prescribe modification strategies that avert the unstable behavior. Whereas conventional Bubble Casting focuses on bubble generation, our work centers on instability theory and mitigating bubble instability.

The Mini-BC technique explains and eliminates the interfacial instability in Bubble Casting milli-SRs, thereby broadening the applicability of Bubble Casting at the millimeter scale. Our study reveals that interfacial tension and viscous resistance generally exert antagonistic effects on interfacial instability when milli-bubble forms in the silicone liquid, a phenomenon not

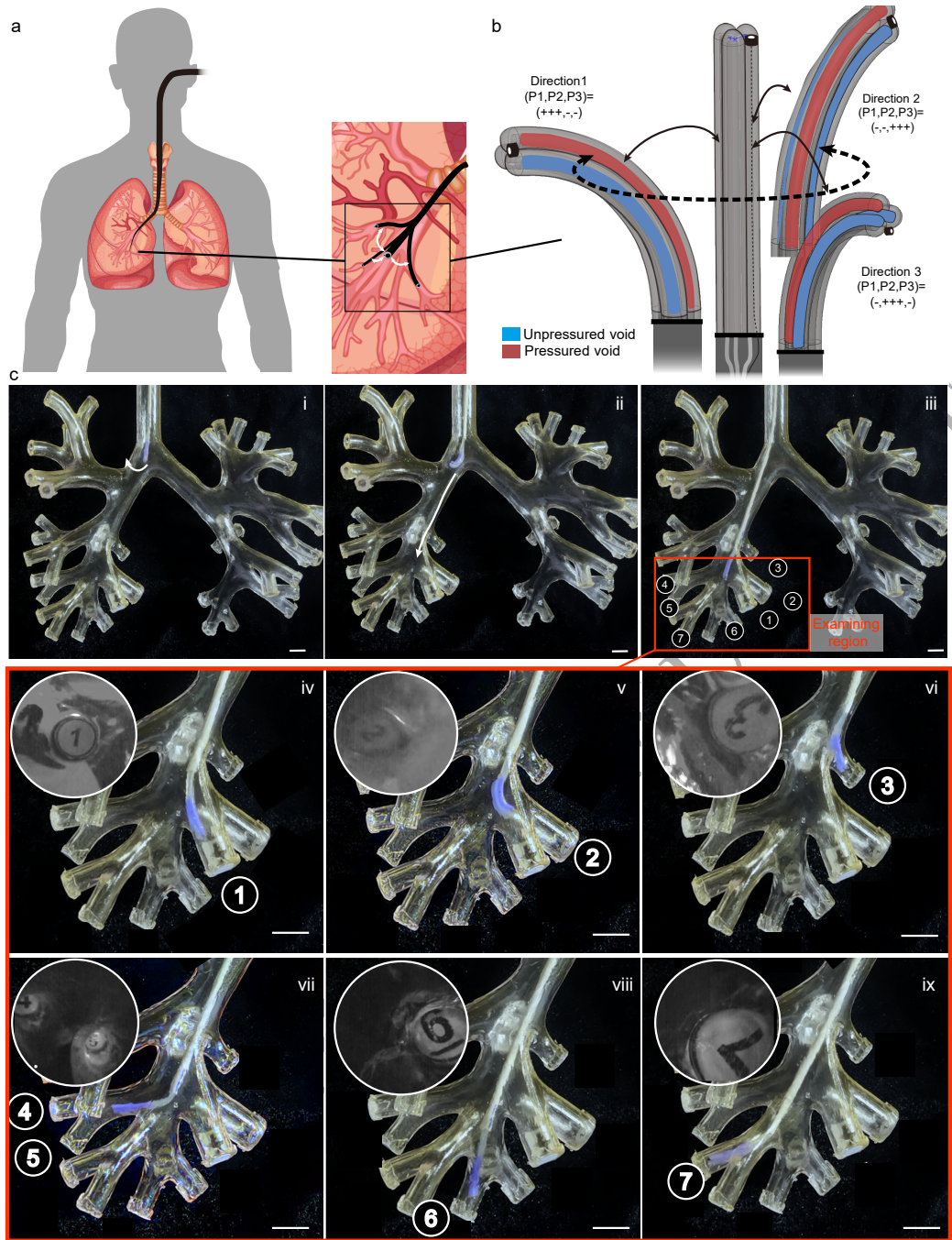


Figure 4: Millimeter-scale soft bronchoscope. (a) Overview of soft bronchoscope steering in the bronchus. (b) The steerable tip has two bending degrees of freedom actuated by three inner pressured voids and the micro-camera captures images from various directions. (c) The soft bronchoscope steers from the trachea (i-ii) to six fourth-order bronchi, (iii-ix) and the micro-camera detects the numbered marks in the endoscopic view on the top-left of each subfigure. Scale bar, 5 mm.

previously addressed in the literature [37,41,42]. Specifically, we propose the critical stable condition  $\tau$  to predict the occurrence of interfacial instability and modification strategies to avoid the interfacial instability. This approach facilitates the fabrication of shape-variable soft robots with dimensions an order of magnitude smaller than

those previously achieved through Bubble Casting. We show the utility of milli-SRs in driving micro-mechanics, grasping tiny objects, and entering narrow tubes. Notably, we present a significant case of a soft bronchoscope that can navigate complex bronchial structures and perform detecting tasks, underscoring the great potential



of Mini-BC milli-SRs in the biomedical field.

Given the versatility of Mini-BC, we will aim to extend its applications across other domains within biomedicine in the future. Coupling milli-SRs with novel materials can extend their capabilities beyond single-elastomer designs, such as shape-memory alloys for tunable stiffness and hydrogel coatings for targeted drug elution. Furthermore, integrating in-situ sensing modules—capable of real-time quantification of temperature, pressure, and chemical composition—into milli-SRs constitutes a pivotal strategy for advancing next-generation process intensification. In summary, our Mini-BC provides a new approach to the design and fabrication of milli-SRs, offering innovative solutions to interfacial instability at the millimeter scale.

## METHOD

### Stability condition

The criterion of stable conditions  $\tau > \tau_{th}$  can be converted into:

Stable state:

$$R > \frac{\tau_{th}}{\beta} \frac{\gamma T_{cure}}{\mu} \quad (5)$$

Unstable state:

$$R < \frac{\tau_{th}}{\beta} \frac{\gamma T_{cure}}{\mu} \quad (6)$$

We mark the stable state with pink and the unstable state with gray in Figure 2e. A linear classifier can separate them with a slope  $\frac{\tau_{th}}{\beta} = 9.1 \times 10^{-4}$ . Therefore, the threshold criterion can be calculated as  $\tau_{th} = 0.3$ .

### Silicone modification

We modify the dual-component platinum cure liquid silicone that is the most commonly used in soft robotics labs. To enhance the class of liquid silicone, such as Dragon Skin 10, Platinum Silicone Cure Accelerator (Plat-Cat) and Thixotropic Agent (Thi-Vex) are chosen. For other kinds of commercial silicone, the corresponding accelerator and thickener can be obtained from silicone suppliers. Additives (Plat-Cat and Thi-Vex) are mixed into Part A of Dragon Skin 10 at weight ratios of 1:20 and 1:100, respectively, using a glass stirring rod. The mixture is then transferred to the left chamber of the cartridge. Subsequently, Part B is poured into another cartridge part, and the silicone cartridge undergoes defoaming in a vacuum chamber (-95 kPa, 20 min). The evacuation rate

should be no more than 10 Pa/s in case of liquid spillage. Following defoaming, we seal the modified silicone into a cartridge with pistons. To mitigate the adverse effects of phase separation in silicone, the sealed cartridge should be stored in a horizontal position to maintain component homogeneity during extrusion. Storage should be at room temperature (73 °F/ 23 °C) away from direct sunlight. To preserve rheological stability, the material should be used within two weeks.

### Injection system

The injection system includes a two-component cartridge gun (MPD50, COX Inc.), cartridges (50ml×50ml, Runze Inc.), and mixing nozzles (F1 XL3.2-16S, Runze Inc.). After installing the mixing nozzle on the cartridge, the cartridge is placed into the gun. Once the gun is triggered, 400 kPa of pressure is applied to extrude both silicone parts into the mixing nozzle in a common weight of 1:1. The initial portion of silicone extruded is recommended to be discarded to avoid issues arising from non-uniform ratios. We connect the nozzle exit and the mold with an elastic silicone tube.

### Rheological protocols

The viscosity of the silicone liquid is characterized by a rotational rheometer (Discovery Hybrid rheometer, TA Instruments Inc.) equipped with a parallel plate. The sample is freshly extruded silicone from the injection system that is thoroughly mixed prior to sampling. The surface tension of the silicone was determined using the drop weight method, with measurements conducted on OCA25 (Dataphysics Instruments Inc.).

### Fabrication of milli-hooker

We fabricate the milli-hooker with silicone (Dragon Skin 10, Smooth on Inc.) in a tubular mold with a diameter of 1.5 mm and a length of 100 mm. The silicone is modified by inserting thickener and accelerator. We propel the bubble in the liquid silicone to the waiting point M and segment #1 forms and rises under the buoyancy (Figure S7a). After waiting time, we propel the bubble to the outlet to form segment #2 of the bubble. The silicone molecules have undergone cross-linking, preventing segment #2 from rising (Figure S7b). Upon curing, the axially variable void enables the milli-actuator to deform into a hook-like shape (Figure S7c).

## SUPPLEMENTARY DATA

Supplementary data are available at NSR online.

## FUNDING

This work was supported in part by the National Natural Science Foundation of China (Grant Nos. 52025057, T2293725, and 52305029), National Key R&D Program of China (Grant No. 2024YFB4707504), the Science and Technology Commission of Shanghai Municipality (Grant No. 24511103400), and Xplorer Prize.

## AUTHOR CONTRIBUTIONS

R.B., N.Z., and G.G. designed research; R.B., N.Z., and X.Y. performed research; G.G. supervised the research; R.B. wrote the manuscript. All authors discussed, reviewed, and edited the manuscript.

**Conflict of interest statement.** None declared.

## REFERENCES

- Kim Y, Parada GA, Liu S *et al.* Ferromagnetic soft continuum robots. *Sci Robot* 2019; **4**: eaax7329.
- Yan Y, Wang T, Zhang R *et al.* Magnetically assisted soft milli-tools for occluded lumen morphology detection. *Sci Adv* 2023; **9**: eadi3979.
- Thai MT, Phan PT, Tran HA *et al.* Advanced soft robotic system for in situ 3D bioprinting and endoscopic surgery. *Adv Sci* 2023; **10**: e2205656.
- Kim Y, Genevriere E, Harker P *et al.* Telerobotic neurovascular interventions with magnetic manipulation. *Sci Robot* 2022; **7**: eabg9907.
- Hu W, Lum GZ, Mastrangeli M *et al.* Small-scale soft-bodied robot with multimodal locomotion. *Nature* 2018; **554**: 81–85.
- Wu Y, Dong X, Kim J *et al.* Wireless soft millirobots for climbing three-dimensional surfaces in confined spaces. *Sci Adv* 2022; **8**: eabn3431.
- Zhang Y, Yang D, Yan P *et al.* Inchworm inspired multimodal soft robots with crawling, climbing, and transitioning locomotion. *IEEE Trans Robot* 2022; **38**: 1806–1819.
- Van Lewen D, Janke T, Lee H *et al.* A millimeter-scale soft robot for tissue biopsy procedures. *Adv Intell Syst* 2023; **5**: 2200326.
- Roh Y, Kim M, Won SM *et al.* Vital signal sensing and manipulation of a microscale organ with a multifunctional soft gripper. *Sci Robot* 2021; **6**: eabi6774.
- Bian R, Zhang N, Yang X *et al.* A variable stiffness soft actuator with a center skeleton and pin-socket jamming layers. *Proc ICIRA (2022)* 325–332.
- Yang Z, Xu C, Lee JX *et al.* Magnetic miniature soft robot with reprogrammable drug-dispensing functionalities: Toward advanced targeted combination therapy. *Adv Mater* 2024; **36**: 2408750.
- Phan PT, Thai MT, Hoang TT *et al.* Hfam: Soft hydraulic filament artificial muscles for flexible robotic applications. *IEEE Access* 2020; **8**: 226637–226652.
- Li Y, Peine J, Mencattelli M *et al.* A soft robotic balloon endoscope for airway procedures. *Soft Robot* 2022; **9**: 1014–1029.
- Diwakar N, Kunti, Miloh T *et al.* AC electrohydrodynamic propulsion and rotation of active particles of engineered shape and asymmetry. *Curr Opin Colloid Interface Sci* 2022; **59**: 101586.
- Lee S, Moghani M, Li A *et al.* A small steerable tip based on dielectric elastomer actuators. *IEEE Robot Autom Lett* 2023; **8**: 6531–6538.
- Dong Y, Wang L, Zhang Z *et al.* Endoscope-assisted magnetic helical micromachine delivery for biofilm eradication in tympanostomy tube. *Sci Adv* 2022; **8**: eabq8573.
- Deng B, Chen L, Wei D *et al.* Pulse-driven robot: Motion via solitary waves. *Sci Adv* 2020; **6**: eaaz1166.
- Son D, Ugurlu MC and Sitti M. Permanent magnet array-driven navigation of wireless millirobots inside soft tissues. *Sci Adv* 2021; **7**: eabi8932.
- Chen X, Goodnight D, Gao Z *et al.* Scaling up nanoscale water-driven energy conversion into evaporation-driven engines and generators. *Nat Commun* 2015; **6**: 8346.
- Fusi G, Del Giudice D, Skarsetz O *et al.* Autonomous soft robots empowered by chemical reaction networks. *Adv Mater* 2023; **35**: 2209870.
- Wang H, Gao J, Xu C *et al.* Light-driven biomimetic nanomotors for enhanced photothermal therapy. *Small* 2024; **20**: 2306208.
- Ahmed S, Wang W, Bai L *et al.* Density and shape effects in the acoustic propulsion of bimetallic nanorod motors. *ACS Nano* 2016; **10**: 4763–4769.
- Gu G, Zhang N, Xu H *et al.* A soft neuroprosthetic hand providing simultaneous myoelectric control and tactile feedback. *Nat Biomed Eng* 2021; **5**: 589–598.
- Polygerinos P, Correll N, Morin SA *et al.* Soft robotics: Review of fluid-driven intrinsically soft devices; manufacturing, sensing, control, and applications in human-robot interaction. *Adv Eng Mater* 2017; **19**: 100016.
- Yang D, Feng M, Sun J *et al.* Soft multifunctional bistable fabric mechanism for electronics-free autonomous robots. *Sci Adv* 2025; **11**: eads8734.
- Zhang N, Ren J, Dong Y *et al.* Soft robotic hand with tactile palm-finger coordination. *Nat Commun* 2025; **16**: 2395.
- Yang X, Zhang N, Huang X *et al.* Multidirectional bending soft pneumatic actuator with fishbone-like strain-limiting layer for dexterous manipulation. *IEEE Robot Autom Lett* 2024; **9**: 3815–3822.
- Kalmar M, Boese A, Landes R *et al.* Injection and infusion technology disruption for use in mri. *Med Dev* 2019; **12**: 469–478.
- Fu S, Dong S, Shen H *et al.* Multifunctional magnetic catheter robot with triaxial force sensing capability for minimally invasive surgery. *Research* 2025; **8**: 0681.
- Shah A and Aran S. A review of magnetic resonance (mr) safety: The essentials to patient safety. *Cureus* 2023; **15**: e47345.
- Ceron S, Gardi G, Petersen K *et al.* Programmable self-organization of heterogeneous microrobot collectives. *Proc Natl Acad Sci USA* 2023; **120**: e2221913120.

32. Yan Y, Wang T, Zhang R *et al.* Magnetically assisted soft milli-tools for occluded lumen morphology detection. *Sci Adv* 2023; **9**: eadi3979.
33. Dong X, Luo X, Zhao H *et al.* Recent advances in biomimetic soft robotics: fabrication approaches, driven strategies and applications. *Soft Matter* 2022; **18**: 7699–7734.
34. Haouas W, Gauthier M and Rabenoroso K. Miniaturized soft robotics: Recent advances and futures opportunities. *Curr Robot Rep* 2024; **5**: 15–27.
35. Chi Y, Zhao Y, Hong Y *et al.* A perspective on miniature soft robotics: Actuation, fabrication, control, and applications. *Adv Intell Syst* 2023; **6**: 20063.
36. Purcell EM. Life at low reynolds number. *Am J Phys* 1977; **45**: 3–11.
37. Fan D, Yuan X, Wu W *et al.* Self-shrinking soft demoulding for complex high-aspect-ratio microchannels. *Nat Commun* 2022; **13**: 32859.
38. Duraivel S, Laurent D, Rajon DA *et al.* A silicone-based support material eliminates interfacial instabilities in 3D silicone printing. *Science* 2023; **379**: 1248–1252.
39. Li J, Cao J, Bian R *et al.* Multimaterial cryogenic printing of three-dimensional soft hydrogel machines. *Nat Commun* 2025; **16**: 185.
40. Ji M, Li Q, Cho IH *et al.* Rapid design and analysis of microtube pneumatic actuators using line-segment and multi-segment euler-bernoulli beam models. *Micromachines* 2019; **10**: 780.
41. Jones TJ, Jambon-Puillet E, Marthelot J *et al.* Bubble casting soft robotics. *Nature* 2021; **599**: 229–233.
42. Becker K, Teeple C, Charles N *et al.* Active entanglement enables stochastic, topological grasping. *Proc Natl Acad Sci USA* 2022; **119**: e2209819119.
43. Guo X, Tang W, Qin K *et al.* Powerful uav manipulation via bioinspired self-adaptive soft self-contained gripper. *Sci Adv* 2024; **10**: eadn6642.
44. Bretherton FP. The motion of long bubbles in tubes. *J Fluid Mech* 1961; **10**: 166.
45. Tsai TM and Miksis MJ. Dynamics of a drop in a constricted capillary tube. *J Fluid Mech* 1994; **274**: 197–217.
46. Olbricht WL and Kung DM. The deformation and breakup of liquid drops in low reynolds number flow through a capillary. *Phys Fluids A* 1992; **4**: 1347–1354.
47. Jang Y, Nabae H and Suzumori K. Effects of surface roughness on direct plasma bonding between silicone rubbers fabricated with 3D-printed molds. *ACS Omega* 2022; **7**: 45004–45013.